2008 IEEE International Conference on
Robotics and Automation
Pasadena, CA, USA, May 19-23, 2008

Stabilization Algorithm for a High Speed Car-Like Robot Achieving Steering Maneuver

E. Lucet [1,2] , Ch. Grand [1] , D. Sallé [2] and Ph. Bidaud [1]
[1] Univsersity of Paris6-UPMC, Institut des Systèmes Intelligents et de Robotique (CNRS - FRE 2507)
{lucet,grand,bidaud}@robot.jussieu.fr
[2] Robosoft, Technopole d'Izarbel, 64210 Bidart
{eric.lucet,damien.salle}@robosoft.fr

Abstract— **This paper deals with design and implementation of a stabilization algorithm for a car like robot performing high speed turns. The control of such a kind of system is rather difficult because of the complexity of the physical wheel-soil interaction model. In this paper, it is planned to analyze the complex dynamic model of this process to elaborate a stabilization algorithm only based on the measurement of the system yaw rate. Finally, a 3D simulation is performed to evaluate the efficiency of this designed stabilization algorithm.**

I. INTRODUCTION

The problem of stabilization of an automated car-like vehicle has been treated in many ways in the literature. The computation of comfortable maneuvers, based on acceleration and jerk constraints, has been studied by Chee and Tomizuka in [1]. The emergency maneuver issue has been addressed in the literature, too. In 1994, Smith and Starkey [2] determined emergency maneuvers by optimizing the gains of a linear controller using the step response of a non linear vehicle model. Then, in 1998, Shiller and Sundar [3] addressed the issue of emergency lane-change maneuvers by the use of a clearance curve, which authorizes to generate shorter maneuvers. In 2006, Spenko [4] presented an algorithm for high speed avoidance based on the organization of a "trajectory space", depending on the vehicle performances. This space is defined by the curvature and the velocity of the car. But, if these papers are focused on the control of kinematic variables as velocity and the generation of trajectory, it is out of the scope of this paper.

We suggest an original not model based stabilization control method for fast autonomous mobile robots, that aims at acting on one of the actuation torques applied to the wheels to reduce the error between desired and measured yaw rate induced by skidding. The overall objective is to follow a given trajectory at relatively high speed by keeping the entire control of the system. In that way, this work can be compared to the electronic stability control (ESC), that appeared in Europe in the 1995 year and was found to have reduced single-vehicle crash involvement risk [5]. The marketing names of ESC systems varying, it is also called electronic stability program (ESP). The major innovation of the algorithm presented here with respect to work dealing with ESP, is that it takes part of a non-linear dynamic model in order to study the influence of forces variation. We make the assumption that the steering angle and the drift angle of the vehicle can be high. Moreover, this algorithm is added to a classical control law for path tracking.

Fig. 1. RobuCAB

The terrains considered here are horizontal and relatively smooth compared to the size of the wheels. If most of the mobile robot motion controllers use the assumption of rolling without slipping, this is no longer suitable at high speed where wheel slip can not be neglected. Due to the dynamics of the vehicle and the saturation of admissible forces by the soil, the slippage reduces the robot motion stability. We propose to analyze the motion control of a class of vehicles that can be represented by the RobuCAB (figure 1), presented in [6]. It is an electric car designed and manufactured by the Robosoft society that consists of a four driven wheels with an Ackerman-style steering system on the front wheels. Each one of the four wheels is independently actuated. If a GPS and odometry are necessary for path tracking, a gyro meter is the only sensor needed for the stabilization algorithm.

This paper is organized as follows. In the second section, the system dynamical model is given. In the third section, we describe the kinematic controller currently implemented on the vehicle and we propose an enhanced controller with the designed stabilization algorithm. In the last section, a 3D simulation is done in a dynamic environment, using a detailed model of wheel-soil interaction forces. The simulations results using this controller are presented and compared to an extended kinematic control law presented by Lenain in [7].

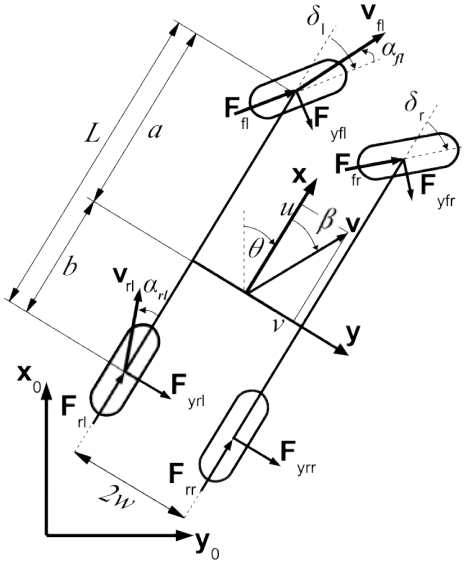

Fig. 2. System parameters

II. System Dynamics Model

A non-linear dynamic model of a car-like nonholonomic vehicle with the front steering wheels is established in fixed frame $[x,y,\theta]^T$, by using the Lagrange method [8]. The vehicle model is described with notations on figure 2. The operationnal space velocity $\left[\dot{x},\dot{y},\dot{\theta}\right]^T$ become $[u,v,r]^T$ in the local framework, linked by the relationship:

$$\begin{bmatrix}\dot{x}\\ \dot{y}\\ \dot{\theta}\end{bmatrix} = \begin{bmatrix}\cos\theta & -\sin\theta & 0\\ \sin\theta & \cos\theta & 0\\ 0 & 0 & 1\end{bmatrix}\cdot\begin{bmatrix}u\\ v\\ r\end{bmatrix} \tag{1}$$

Let us denote δ_l and δ_r the left anf right steering angles of the front wheels. The slippage angles are denoted α_{**} (with f and r for front and rear, and l and r for left and right). These angles express the difference between the direction of the expected wheel velocities and the real direction of the vehicle velocities at each contact point. The wheel-ground interaction forces are F_{**} and F_{y**} for each one of the four wheels in both the longitudinal **x** and the lateral **y** directions.

Dynamical model of this nonholonomic system, by neglecting the torques due to wheels steering motion, can be described by the following equations:

$$\left\{\begin{array}{rcl} M(\dot{u}-rv) &=& F_{rl}+F_{rr}+F_{fl}\cos\delta_l+F_{fr}\cos\delta_r\\ && -F_{yfl}\sin\delta_l-F_{yfr}\sin\delta_r\\ M(\dot{v}+ru) &=& F_{yrl}+F_{yrr}+F_{yfl}\cos\delta_l+F_{yfr}\cos\delta_r\\ && +F_{fl}\sin\delta_l+F_{fr}\sin\delta_r\\ J\dot{r} &=& wF_{rl}-bF_{yrl}-wF_{rr}-bF_{yrr}\\ && +F_{fl}(a\sin\delta_l+w\cos\delta_l)\\ && +F_{yfl}(a\cos\delta_l-w\sin\delta_l)\\ && +F_{fr}(a\sin\delta_r-w\cos\delta_r)\\ && +F_{yfr}(a\cos\delta_r+w\sin\delta_r)\end{array}\right. \tag{2}$$

Where M and J are the mass and the inertia of the vehicle.

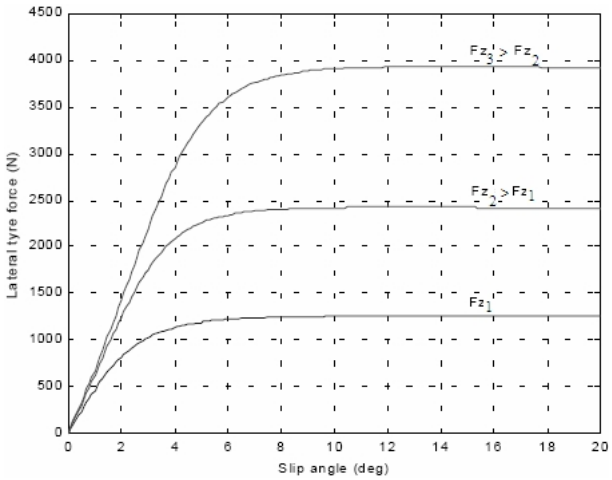

Fig. 3. Empirical model of lateral force vs slip angle (adapted from [9])

Based on the schema described in figure 2, we have the kinematic relationships:

$$\begin{array}{c}\tan(\delta_r-\alpha_{fr})=\frac{ar+v}{u-rw}\ ;\ \tan(\delta_l-\alpha_{fl})=\frac{ar+v}{u+rw}\ ;\\ \tan\alpha_{rr}=\frac{br-v}{u-rw}\ ;\ \tan\alpha_{rl}=\frac{br-v}{u+rw}.\end{array} \tag{3}$$

If we consider that the slip angles are small enough, so we have:

$$\begin{array}{ccc}\alpha_{fr}\approx\delta_r-\frac{ar+v}{u-rw} & ; & \alpha_{fl}\approx\delta_l-\frac{ar+v}{u+rw}\ ;\\ \alpha_{rr}\approx\frac{br-v}{u-rw} & ; & \alpha_{rl}\approx\frac{br-v}{u+rw}.\end{array} \tag{4}$$

Furthermore, it has been shown (see figure 3) [9] that, for one given type of tire and one given vertical force (F_z), for a slip angle small enough, there is a proportional link between the lateral force and this slip angle. So, $C_{\alpha**}$ being a strictly positive constant, we can write for the four wheels:

$$F_{y**}=C_{\alpha**}\alpha_{**} \tag{5}$$

Therefore, the dynamic equations (2), when satisfying equations (4) and (5), can be reformulated as

$$\left\{\begin{array}{rcl} M(\dot{u}-rv) &=& F_{rl}+F_{fl}\cos\delta_l+F_{rr}+F_{fr}\cos\delta_r\\ && -C_{\alpha fl}\left(\delta_l-\frac{ar+v}{u+rw}\right)\sin\delta_l\\ && -C_{\alpha fr}\left(\delta_r-\frac{ar+v}{u-rw}\right)\sin\delta_r\\ M(\dot{v}+ru) &=& C_{\alpha rl}\left(\frac{br-v}{u+rw}\right)+C_{\alpha rr}\left(\frac{br-v}{u-rw}\right)\\ && +C_{\alpha fl}\left(\delta_l-\frac{ar+v}{u+rw}\right)\cos\delta_l\\ && +C_{\alpha fr}\left(\delta_r-\frac{ar+v}{u-rw}\right)\cos\delta_r\\ && +F_{fl}\sin\delta_l+F_{fr}\sin\delta_r\\ J\dot{r} &=& -bC_{\alpha rl}\left(\frac{br-v}{u+rw}\right)-bC_{\alpha rr}\left(\frac{br-v}{u-rw}\right)\\ && +F_{fl}(a\sin\delta_l+w\cos\delta_l)+wF_{rl}\\ && +F_{fr}(a\sin\delta_r-w\cos\delta_r)-wF_{rr}\\ && +C_{\alpha fl}\left(\delta_l-\frac{ar+v}{u+rw}\right)(a\cos\delta_l-w\sin\delta_l)\\ && +C_{\alpha fr}\left(\delta_r-\frac{ar+v}{u-rw}\right)(a\cos\delta_r+w\sin\delta_r)\end{array}\right. \tag{6}$$

The dynamics equation (6) can be written in more compact matrix form as:

$$\mathbf{D}\dot{\mathbf{u}}+\mathbf{C}(\mathbf{u})\mathbf{u}=\mathbf{B}\tau+\mathbf{J}^{\mathbf{T}}\lambda \tag{7}$$

Where the inertial matrix is:

$$\mathbf{D} = \begin{pmatrix} M & 0 & 0 \\ 0 & M & 0 \\ 0 & 0 & J \end{pmatrix}$$

The Coriolis matrix is:

$$\mathbf{C}(\mathbf{u}) = \begin{pmatrix} 0 & -Mr & 0 \\ Mr & 0 & 0 \\ 0 & 0 & 0 \end{pmatrix}$$

The input transformation matrix is:

$$\mathbf{B} = \begin{pmatrix} \cos\delta_l & \cos\delta_r & 1 & 1 \\ \sin\delta_l & \sin\delta_r & 0 & 0 \\ w\cos\delta_l + a\sin\delta_l & -w\cos\delta_r + a\sin\delta_r & w & -w \end{pmatrix}$$

Here, the vector of vehicle velocities expressed in the local frame is:

$$\mathbf{u} = \begin{pmatrix} u & v & r \end{pmatrix}^T$$

In this plant, the input vector includes the forces applied to each one of the four wheels:

$$\tau = \begin{pmatrix} F_{fl} & F_{fr} & F_{rl} & F_{rr} \end{pmatrix}^T$$

The steering angle δ is handled as a static parameter and will be controlled independently. λ is the associated Lagrangian multipliers which expresses the lateral force on the wheel-soil contact point. The longitudinal contact forces, which have to be taken into account [10], are not considered here because they are already included in the input vector.

$$\lambda = \begin{pmatrix} C_{\alpha fl}\left(\delta_l - \frac{ar+v}{u+rw}\right) \\ C_{\alpha fr}\left(\delta_r - \frac{ar+v}{u-rw}\right) \\ C_{\alpha rl}\left(\frac{br-v}{u+rw}\right) \\ C_{\alpha rr}\left(\frac{br-v}{u-rw}\right) \end{pmatrix}$$

The constraint matrix is:

$$\mathbf{J} = \begin{pmatrix} -\sin\delta_l & \cos\delta_l & a\cos\delta_l - w\sin\delta_l \\ -\sin\delta_r & \sin\delta_r & a\cos\delta_r + w\sin\delta_r \\ 0 & 1 & -b \\ 0 & 1 & -b \end{pmatrix}$$

We notice that:

$$\mathbf{J}\mathbf{u} = \begin{pmatrix} -u\sin\delta + v\cos\delta_l + r(a\cos\delta_l - w\sin\delta_l) \\ -u\sin\delta + v\cos\delta_r + r(a\cos\delta_r + w\sin\delta_r) \\ v - r\mathrm{b} \\ v - r\mathrm{b} \end{pmatrix}$$

Based on (3), we have:

$$\mathbf{J}\mathbf{u} = \begin{pmatrix} (u+\mathrm{wr})\left(-\sin\delta_l + \cos\delta_l \tan\left(\delta_l - \alpha_{fl}\right)\right) \\ (u-\mathrm{wr})\left(-\sin\delta_r + \cos\delta_r \tan\left(\delta_r - \alpha_{fr}\right)\right) \\ -(u+wr)\,tan\alpha_{rl} \\ -(u-wr)\,tan\alpha_{rr} \end{pmatrix}$$

If we make the hypothesis of rolling without slipping, so we suppose that for each wheel $\alpha_{**} = 0$ and we obtain:

$$\mathbf{J}\mathbf{u} = \mathbf{0}$$

This is the nonholonomic constraint equation.

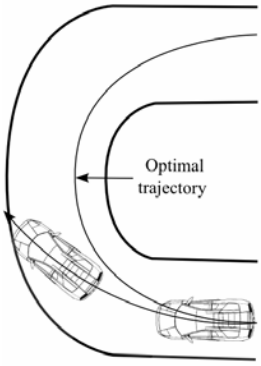

Fig. 4. Understeering

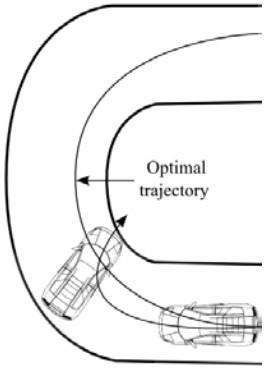

Fig. 5. Oversteering

III. Design of motion controller

A. Basic kinematic controller and limitations

The currently implemented controller on the plant is a standard velocity controller. When turning, the desired velocity is constant at $4ms^{-1}$. The torque applied to the wheels is determined by the low level control:

$$\Gamma = K_C\,(V_d - R\omega)$$

Where K_C is a strictly positive constant, V_d the desired velocity, R the radius of the wheels and ω the mean angular velocity of the axis of the wheels. Here: $K_C = 200Ns$.

The steer angle of the robot vehicle is determined by the kinematic control:

$$\delta = K_P\varepsilon_{lateral} + K_E\varepsilon_{heading}$$

With $\varepsilon_{lateral}$ the lateral error (in meters), $\varepsilon_{heading}$ the heading error (in radians), and K_P and K_E, two strictly positive gains. K_E is a constant and K_P is defined as : $K_P = K_{P1}e^{-K_{P2}\|\mathbf{V}\|}$, with K_{P1} and K_{P2} two strictly positive constants.

We can see that a car-like vehicle understeers (figure 4) when the front wheels are going outside of the curvature, i.e. the front wheels are slipping more than the rear ones. In that case, there is a hazard of ram off roadway accident.

In the same way, a car-like vehicle oversteers (figure 5) when the rear wheels are going outside of the curvature, i.e. the rear wheels are slipping more than the front ones. In that case, there is a hazard of swing-around.

Considering that a tracking control is already used in order to determine the velocity and the steering of the vehicle, we design a stabilization algorithm to avoid the two phenomena of under and oversteering, keeping the controllability of it.

The control objective can be specified as follows. Given a desired yaw rate r_d and measuring the real yaw rate r with a gyrometer, determine a law for τ such that the controllability of the vehicle is guarantied when turning.

To solve this problem, we apply a negative force on one of the four wheels to counter the slippage and keep the adhesion

of the wheels in the soil. For that, we study the influence of different parameters, and consider the yaw rate error:

$$\varepsilon = r_d - r$$

B. Study of the influence of the controllable parameters

Based on the dynamics equation (6), we can study the effect of the controllable parameters F_{fl}, F_{fr}, F_{rl} and F_{rr} on the global force and torque of the system. The values of the steering angles of the front wheels δ_l and δ_r are defined as $(\delta_l, \delta_r) \in \left]-\frac{\pi}{2}; \frac{\pi}{2}\right]^2$. As a result, $\cos\delta_l \geq 0$, $\cos\delta_r \geq 0$ and, in order to determine the sign of $\sin\delta_l$ and $\sin\delta_r$, we have to know the value of δ_l and δ_r.

Influence of F_{fl}:
- Following the axis x: $\frac{dF_x}{dF_{fl}} = \cos\delta_l$. The force increases.
- Following the axis y: $\frac{dF_y}{dF_{fl}} = \sin\delta_l$.
  . If $\delta_l < 0$: the force decreases.
  . If $\delta_l = 0$: no influence.
  . If $\delta_l > 0$: the force increases.
- Following θ: $\frac{dM_\theta}{dF_{fl}} = a\sin\delta_l + w\cos\delta_l$.
  . If $\delta_l < \arctan(\frac{-w}{a})$: the torque decreases.
  . If $\delta_l = \arctan(\frac{-w}{a})$: no influence.
  . If $\delta_l > \arctan(\frac{-w}{a})$: the torque increases.

Influence of F_{fr}:
- Following the axis x and y: idem F_{fl}.
- Following θ: $\frac{dM_\theta}{dF_{fr}} = a\sin\delta_r - w\cos\delta_r$.
  . If $\delta_r < \arctan(\frac{w}{a})$: the torque decreases.
  . If $\delta_r = \arctan(\frac{w}{a})$: no influence.
  . If $\delta_r > \arctan(\frac{w}{a})$: the torque increases.

Influence of F_{rl}:
- Following the axis x: $\frac{dF_x}{dF_{rl}} = 1$. The force increases.
- Following the axis y: $\frac{dF_y}{dF_{rl}} = 0$. No influence.
- Following θ: $\frac{dM_\theta}{dF_{rl}} = w$. The torque increases.

Influence of F_{rr}:
- Following the axis x and y: idem F_{rl}.
- Following θ: $\frac{dM_\theta}{dF_{rr}} = -w$. The torque decreases.

C. Study summary

Then, we can recap the results of this study in the table I.

We notice that for a skid-steering vehicle ($\delta = 0$), we can't control its lateral dynamic. And, like expected, the fluctuations of the steer angle have no consequence at the influence of the rear wheels (F_{rl} and F_{rr}).

We remind that the signs of δ_l, δ_r and δ are always the same, and they are relied by the relationships:

$$\cot\delta_l = \cot\delta - \frac{W}{L'} \quad ; \quad \cot\delta_r = \cot\delta + \frac{W}{L'}$$

δ is the steering angle theoritically equivalent to the bicycle model (without slippage) and L' is a stricly positive constant with a value depending on the slippage angles. If there is no slippage ($\alpha_{**} = 0$), $L' = L$. Considering the yaw rate r, we have:

$$u = r/\rho \tag{8}$$

where ρ is the curvature of the curve. And we have the other relationship:

$$\tan\delta = L\rho \tag{9}$$

Considering (8) and (9) we obtain:

$$r = u\frac{\tan\delta}{L} \tag{10}$$

Then, using (10), we can measure the steering angle δ and the longitudinal velocity u of the vehicle and knowing the desired yaw rate r_d in real time. If the vehicle is slipping, the equation becomes [11]:

$$r = u\cos\alpha_r \frac{\tan\left(\delta + \alpha_f\right) - \tan\alpha_r}{L} \tag{11}$$

So, the value of r is different and if ε (the yaw rate error) becomes too high, the vehicle can be no more controllable. Then, to determine the behavior of the robot, we have to distinguish if it turns in the positive or in the negative θ direction.

TABLE I
STUDY SUMMARY

		F_{fl}	F_{fr}	F_{rl}	F_{rr}
F_x		+	+	+	+
F_y	$\delta_l \leq \delta \leq \delta_r < 0$	−	−		
	$\delta = \delta_l = \delta_r = 0$	=	=	=	=
	$\delta_r \geq \delta \geq \delta_l > 0$	+	+		
M_θ	$\delta_l < \arctan(\frac{-w}{a})$	−	−		
	$\delta_l = \arctan(\frac{-w}{a})$	=	−		
	$\arctan(\frac{-w}{a}) < \delta_l \leq \delta \leq \delta_r < \arctan(\frac{w}{a})$	+	−	+	−
	$\delta_r = \arctan(\frac{w}{a})$	+	=		
	$\delta_r > \arctan(\frac{w}{a})$	+	+		

D. Turn in the positive θ direction

In that case, r_d and δ are positive values. After measuring r, we deduce the sign of ε. If $\varepsilon < 0$, the value of r is too high, meaning that the vehicle oversteers. We have to decrease the value of the torque M_θ . Based on the table I, we see that we can apply a negative force in the left front wheel F_{fl} or in the left rear wheel F_{rl}. But F_{fl} permits a lateral displacement following $-\mathbf{y}$ ($F_y = F_{fl}\sin\delta_l$), that permits a better stability. So we apply a negative force F_{fl}. If $\varepsilon > 0$, the value of r is too small, meaning that the vehicle understeers. We have to increase the value of the torque M_θ. Based on the table I, we see that we can apply a negative force in the right rear wheel F_{rr} or in the right front wheel F_{fr}. But with F_{fr}, the value of M_θ increases only if $\delta_r < \arctan(\frac{w}{a})$ and with less efficiency than F_{rr}. Furthermore, the lateral displacement ($F_y = F_{fr}\sin\delta_r$) is undesirable. So we apply a negative force F_{rr}.

E. Turn in the negative θ direction

In that case, r_d and δ are negative values. After measuring r, we deduce the sign of ε. If $\varepsilon < 0$, the value of r is too small, meaning that the vehicle understeers. We have to decrease le value of the torque M_θ. Based on the table I, we see that we can apply a negative force in the left rear wheel F_{rl}. So we apply a negative force F_{rl}. If $\varepsilon > 0$, the value of r is too high, meaning that the vehicle oversteers. We have to increase the value of the torque M_θ. Based on the table I, we see that we can apply a negative force in the right rear wheel F_{rr} or in the right front wheel F_{fr}. But F_{fr} allows a lateral displacement ($F_y = F_{fr}\sin\delta_r$), that permits a better stability. So we apply a negative force F_{fr}.

F. Algorithm summary

If $\delta < 0$
  If $\varepsilon < -\ limit$
    Negative force F_{rl} *applied.*
  End $\varepsilon < -\ limit$
  If $\varepsilon > limit$
    Negative force F_{fr} *applied.*
  End $\varepsilon > limit$
End $\delta < 0$
If $\delta > 0$
  If $\varepsilon < -\ limit$
    Negative force F_{fl} *applied.*
  End $\varepsilon < -\ limit$
  If $\varepsilon > limit$
    Negative force F_{rr} *applied.*
  End $\varepsilon > limit$
End $\delta > 0$

For each of the different cases, the value of the force applied is chosen such as:

$$F = -K|\varepsilon| \tag{12}$$

And it is applied to adequate wheel with respect to the previous algorithm. Here K is a strictly positive constant, depending of the nature of the soil. The limit on ε permits to determine the threshold of activation of this stabilization control.

IV. Simulation

The simulation is led with the dynamics model of the robuCAB, having the properties done in table II.

The simulation was performed using Ageia PhysX [12], an highly realistic 3-dimensional dynamic environment. An advanced tire slip based friction model from a Szostak, Allen and Rosenthal paper ([13], [14]), explained in [15], is used in this simulator. It separates the overall friction force into longitudal and lateral components. It is represented by the function depicted in 6, the force being in N and the composite slip, taking into account the longitudinal slip of the tire and the slip angle, without unity. We use here the following parameters:

. Coordinates of the extremum point A: $(1.0; 0.02)$;
. Coordinates of the point B, beginning of the Asymptote: $(2.0; 0.01)$;
. Longitudinal stiffness factor $= 10^5$;
. Lateral stiffness factor $= 10^5$.

TABLE II
Robot Properties

Description	Symbol	Value
Length of the vehicle	L	2.1 m
Width of the vehicle	2w	1.2 m
Distance between the front wheel and the centre of gravity	a	1.1 m
Distance between the rear wheel and the centre of gravity	b	1.0 m
Mass of the vehicle	M	500 Kg
Inertia of the vehicle	J	244 $Kg \cdot m^2$

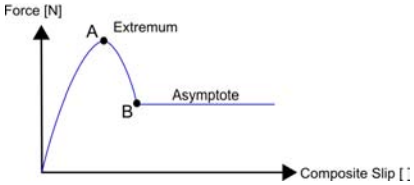

Fig. 6. Friction model

The stiffness factor is the base amount of "grip" the tire has in the specified direction. We can adjust the stiffness and tire force curve to taste to tweak the conditions under which the tires start to skid and when they regain traction with the ground.

The controller parameters are chosen as: $K_{P1} = 2m^{-1}$, $K_{P2} = 1sm^{-1}$, $K_E = 1$ and, for the stabilization algorithm: $K = 60Ns$ and $limit = 0.4rad.s^{-1}$.

As we can see in 7, our approach consists in adapting the couples applied in the axis of the wheels with the added algorithm designed in IV. The equation (10) is used in order to determine the desired yaw rate r_d.

After having reached a velocity of $4ms^{-1}$, the simulation consists of following a sinusoidal path. In figure 8, the trajectory of the cart is displayed with and without stabilization, and with an extended kinematic control law [7] that takes into account the sliding phenomena. In figure 9, the yaw rate error during the simulations with and without stabilization is

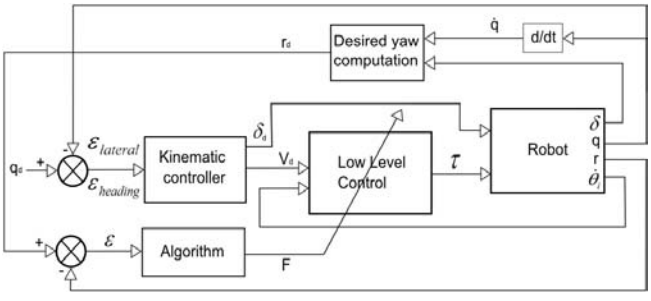

Fig. 7. Control block diagram

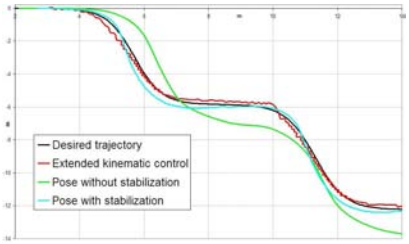

Fig. 8. Pose of the robot

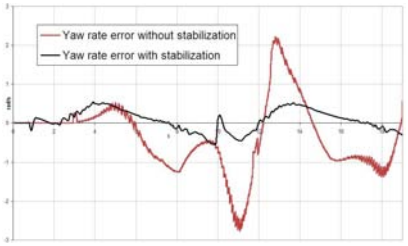

Fig. 9. Yaw rate error (ε)

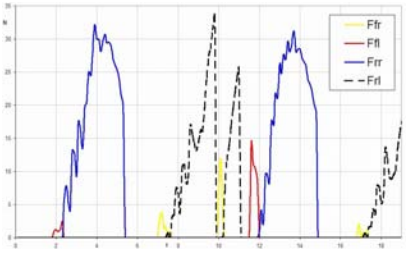

Fig. 10. Applied forces with stabilization

displayed in $rad.s^{-1}$. And, in figure 10, the applied forces during the car displacements with stabilization are displayed in N. At first, turning in the positive θ direction , we see figure 8 that without stabilization, the vehicle understeers. As a consequence, a positive yaw rate error can be seen figure 9. With the stabilization algorithm, we see figure 10 a negative force of about $34N$ applied in the rear right wheel to prevent it. Then, when the vehicle is turning in the negative θ direction, it understeers, so the yaw rate becomes negative and a negative force of about $37N$ is applied in the rear left wheel. At $t = 10s$ we see in figure 9 that the yaw rate error curvature with stabilisation becomes briefly positive, what explains a negative force of about $12N$ applied in the front right wheel. When the vehicle restart to turn in the positive θ direction, there is a little negative yaw rate error, so a negative force of about $15N$ is applied in the front left wheel. Finally, we observe again the two first phenomena.

Eventually, our control law is compared to the extended kinematic control law. The displacements of the robot show figure 8 that this control law, with the parameters correcly adjusted, authorizes to be very close to the path. But it is unstable, because the vehicle is oscillating. With different control settings, we can minimize the oscillations, but the path will no more be followed correctly.

In conclusion, this simulation shows that the stabilization controller has good performance in term of tracking error and yaw stability because it can well reduce the yaw rate error to avoid the oversteering and understeering phenomena.

V. Conclusions

Control of a car-like robot is the source of many difficulties because of the unknown of the wheel-soil interaction. This algorithm has the advantage to avoid it by using only the knowledge of the yaw rate of the vehicle. The simulation in a realistic dynamic environment has shown its efficiency. Eventually, this algorithm could be completed with a 3D dynamic model [16] and used in an unstructured environment in order to investigate the influence of sensor noise, specially the gyro drift.

References

[1] M. Tomizuka W. Chee. Lane change maneuver of automobiles for the intelligent vehicle and highway system (ivhs). In *American Control Conference*, pages 3586–3587, June 1994.

[2] J.M. Starkey D.E. Smith. Effects of model complexity on the performance of automated vehicle steering controller: controller development and evaluation. *Journal of Vehicle System Dynamics*, 23:627–645, 1994.

[3] S. Sundar Z. Shiller. Emergency lane-change maneuvers of autonomous vehicles. *Journal of Vehicle Dynamic Systems, Measurement, and Control*, 120:37–44, March 1998.

[4] M. Spenko, Y. Kuroda, S. Dubowsky, and K. Iagnemma. Hazard avoidance for high-speed mobile robots in rough terrain. *Journal of Field Robotics*, May 2006.

[5] Charles M. Farmer. Effects of electronic stability control:an update. *Traffic Injury Prevention*, 7:4:319 – 324, 2006.

[6] C. Torras G. Alenyà, E. Martinez. Fusing visual and inertial sensing to recover robot ego-motion. *Journal of Robotic Systems*, 21(1):2332, 2004.

[7] R. Lenain, B. Thuilot, C. Cariou, and P. Martinet. High accuracy path tracking for vehicle in presence of sliding: Application to farm vehicles automatic guidance for agricultural task. *Autonomous Robots*, pages 79–97, 2006.

[8] G. Campion, B. d'Andréa-Novel, and G. Bastin. Controllability and state feedback stabilization of nonholonomic mechanical systems. *Advanced Robot Control, Lecture Notes in Control and Information Sciences*, 162:106–124, 1990.

[9] Hans B. Pacejka. *Tyre and vehicle dynamics*. Ed. Elsevier Butterworth-Heinemann, 2002.

[10] D. Lhomme-Desages, Ch. Grand, and J.C. Guinot. Trajectory control of a four-wheel skid-steering vehicle over soft terrain using a physical interaction model. In *Proceedings of ICRA'07 : IEEE/Int. Conf. on Robotics and Automation*, pages 1164 – 1169, Roma, Italy, April 2007.

[11] R. Lenain. *Contribution à la modélisation et à la commande de robots mobiles en présence de glissements*. PhD thesis, Université Blaise Pascal Clermont II (France), 14 novembre 2005.

[12] Jeff Craighead, Robin Murphy, Jenny Burke, and Brian Goldiez. A survey of commercial & open source unmanned vehicle simulators. In *Proceedings of ICRA'07 : IEEE/Int. Conf. on Robotics and Automation*, pages 852–857, Roma, Italy, April 2007.

[13] H.T. Szostak, W.R. Allen, and T.J. Rosenthal. Analytical Modeling of Driver Response in Crash Avoidance Maneuvering Volume II: An Interactive Model for Driver/Vehicle Simulation. U.S Department of Transportation Report NHTSA DOT HS-807-271, April 1988.

[14] Control, Dynamics, & Estimation Laboratory at SUNY at Buffalo. [Online]. Available: http://code.eng.buffalo.edu/dat/sites/tire/tire.html. *Tire Model in Driving Simulator.*

[15] Copyright 2006 AGEIA Technologies Inc, Suite 118, 82 Pioneer Way, Mountain View, CA 94041 U.S.A. All rights reserved. www.ageia.com. *AGEIA PhysX Documentation, NxTireFunctionDesc Class Reference*.

[16] M. Pham. Modélisation mathématique du comportement dynamique d'une automobile dans le domaine non linéaire. *Revue de la Société des Ingénieurs Automobile*, 40, 1986.